

Perovskite-Type Oxynitride Nanofibers Performing Photocatalytic Oxygen and Hydrogen Generation

Anja Hofmann, Morten Weiss, Jana Timm, and Roland Marschall*

Ba₅Nb₄O₁₅ nanofibers with tailored nanofiber diameters are prepared via electrospinning, and treated in ammonia gas to synthesize niobate oxynitride nanofibers. Most importantly, the nanofibers retain their fiber morphology during ammonolysis, and the nanofiber diameter of the converted fibers can be adjusted. Only a thorough characterization, including detailed Rietveld refinements, can reveal that the ammonolysis of Ba₅Nb₄O₁₅ results not only in BaNbO₂N, but also generates Ba₂NbO₃N as additional oxynitride phase. Such BaNbO₂N–Ba₂NbO₃N composite nanofibers with adjusted nanofiber diameters are applied in photocatalytic water oxidation and hydrogen generation. After decoration with CoNbO₄ or Pt cocatalyst, the materials show a diameter-dependent photocatalytic activity, respectively, with an optimum nanofiber diameter. The presented synthesis demonstrates a novel sol–gel-derived possibility for nanostructuring of oxynitrides, which can pave the way for new synthesis strategies of nanostructured complex oxynitrides.

for water oxidation and reduction.^[7–11] For comparison, other oxynitrides such as SrNbO₂N with an absorption edge at 700 nm,^[1] BaTaO₂N at 660 nm,^[4] LaTiO₂N at 600 nm,^[2] and CaTaO₂N at 510 nm^[3] show less pronounced visible-light absorption. This makes BaNbO₂N a very interesting semiconductor material for visible-light photocatalytic and photoelectrochemical water splitting.^[8–10,12–14] BaNbO₂N can be synthesized by different synthesis routes, solid-state reaction route by ammonolysis of a mixture of BaCO₃ and Nb₂O₅ is one prominent example.^[5,6,13,15,16] Odahara et al. synthesized BaNbO₂N by an intense exothermic and explosive reaction without the need of a nitridation step.^[17] Other routes include an additional step with the synthesis of an oxide precursor, such as BaNbO₃ or


the layered perovskite Ba₅Nb₄O₁₅ or an amorphous oxide precursor, which is subsequently nitrided.^[7,9–14,18,19] Hojamberdiev et al. prepared BaNbO₂N crystals via a NH₃-assisted flux-growth approach by ammonolysis of a mixture of BaCO₃ and Nb₂O₅ and KCl.^[8] Hisatomi et al. showed a faster ammonia flow and a higher barium to niobium ratio in the precursor results in a suppressed niobium reduction.^[13] Furthermore, they reported an increase in the photocatalytic activity by using precursors prepared via a soft chemistry route, compared to a mixture of BaCO₃ and Nb₂O₅ due to a lower nitridation temperature.^[13] A nitridation of size-controlled Ba₅Nb₄O₁₅ crystals in micrometer size was reported by Yamada et al. and they assumed that the differences in photocatalytic activity can be assigned to competitive effects of crystallinity and anion deficiency in the prepared size-controlled BaNbO₂N.^[10]

All aforementioned syntheses—excluding the explosive reaction—include a nitridation step at high temperature (1023 to 1273 K), which often leads to micrometer-sized particles and therefore small surface areas with resulting poor catalyst-reactant contact-areas. The catalyst surface could be increased by nanostructuring. The already mentioned, necessary high temperatures hamper the classical nanostructuring routes via surfactants or templated sol–gel chemistry. An advanced technique to overcome the problem of rapid crystal growth is electrospinning, which is very often used in polymer science, but is also suitable for the preparation of metal oxides such as Ba₅Nb₄O₁₅ and Ba₅Ta₄O₁₅.^[20,21] The advantage of using electrospinning is the resulting fiber morphology after the spinning process. Even the required crystallization preserves the fiber morphology.^[20] Furthermore, it is possible to synthesize metal oxides such as Ba₅Nb₄O₁₅ with a reduced temperature

1. Introduction

Due to ever-growing energy demand, research for generating renewable, clean hydrogen by using solar-light-induced water splitting becomes more important. The most crucial part of an (solar-light driven) efficient water splitting process is a suitable catalyst/cocatalyst system: any photocatalytically active material is highly dependent on band positions and optical bandgap. First, the band positions of the semiconducting photocatalyst have to be suitable for water splitting. Further, to achieve a high solar-to-hydrogen efficiency a semiconductor has to absorb a wide range of visible light. Perovskite-oxynitrides AB(O,N)₃ (A = La, Ca, Sr, or Ba; B = Ti, Ta, Nb) are fulfilling these requirements.^[1–4] BaNbO₂N (*Pm* $\bar{3}m$),^[5,6] for example, shows superior visible-light absorption up to 740 nm, corresponding to a bandgap of 1.7 to 1.8 eV, compared to other perovskite oxynitrides, and suitable band positions

A. Hofmann, Dr. M. Weiss, Dr. J. Timm, Prof. R. Marschall
Department of Chemistry
University of Bayreuth
Universitätsstraße 30, 95447 Bayreuth, Germany
E-mail: roland.marschall@uni-bayreuth.de

 The ORCID identification number(s) for the author(s) of this article can be found under <https://doi.org/10.1002/admi.202100813>.

© 2021 The Authors. Advanced Materials Interfaces published by Wiley-VCH GmbH. This is an open access article under the terms of the Creative Commons Attribution License, which permits use, distribution and reproduction in any medium, provided the original work is properly cited.

DOI: 10.1002/admi.202100813

(800–900 °C) compared to the solid-state reaction synthesis (up to 1500 °C).^[20,22] Moreover, the nanofiber diameter of the resulting oxide can be tuned by adjusting the viscosity of the spinning solution, as reported for Ba₅Ta₄O₁₅ nanofibers and Ba₅Ta₄O₁₅–Ba₃Ta₅O₁₅ composite nanofibers.^[21,23] Bloesser et al. were able to show a nanofiber diameter dependent activity in photocatalytic overall water splitting for Ba₅Ta₄O₁₅ with an optimum nanofiber diameter of 161 nm.^[21]

Here, we present the first study to prepare diameter-controlled oxynitride nanofibers of BaNbO₂N by electrospinning. We combine the reported positive effect of a Ba/Nb ratio >1^[13] with the positive effect of the electrospinning to boost the photocatalytic activity of BaNbO₂N. Fully crystalline Ba₅Nb₄O₁₅ nanofibers with adjusted diameters are synthesized via sol–gel electrospinning, and converted to corresponding BaNbO₂N nanofibers. Morphology and detailed bulk and surface analysis of the prepared BaNbO₂N samples are provided, showing the formation of a Ba₂NbO₃N–BaNbO₂N composite. The nanofiber morphology and diameter retain nicely during the nitridation of the Ba₅Nb₄O₁₅ nanofibers. Diameter-dependent hydrogen and oxygen evolution results are presented, and overall water splitting activity is investigated on the most active sample.

2. Results and Discussion

2.1. Characterization

Scanning electron microscopy (SEM) images of the nitrated nanofibers (N-NFs) of different diameter are shown in **Figure 1**. All samples still exhibit the nanofiber morphology after the ammonolysis of Ba₅Nb₄O₁₅ precursor nanofibers. Figure S1 of the Supporting Information shows for one exemplary sample that

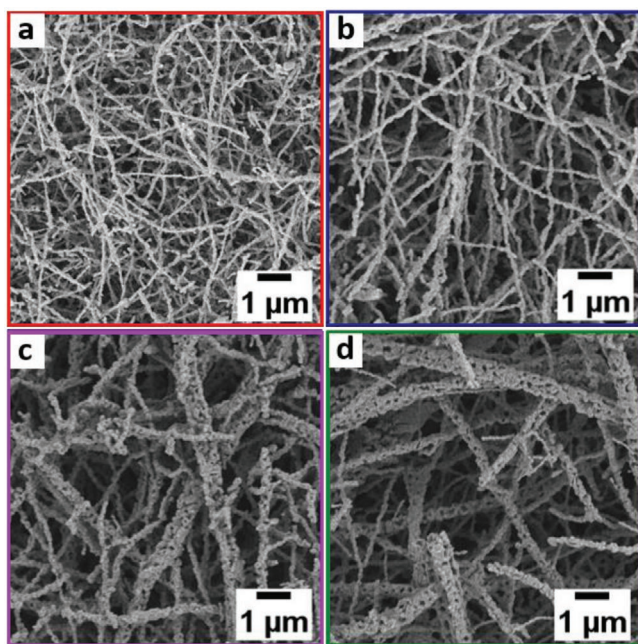


Figure 1. SEM images of N-NF with nanofiber diameters of a) 135 nm, b) 156 nm, c) 194 nm, and d) 213 nm.

Table 1. Nanofiber diameter and BET surface area of Ba₅Nb₄O₁₅ nanofibers and converted N-NF depending on the amount of PVP used for electrospinning.

Amount of PVP [mg]	Average nanofiber diameter of Ba ₅ Nb ₄ O ₁₅ [nm]	Average nanofiber diameter of N-NF [nm]	BET surface area [m ² g ⁻¹]
200	109 ± 39	135 ± 44 ^{a)}	8.2 ^{b)}
300	157 ± 58	156 ± 61 ^{a)}	7.1 ^{b)}
400	169 ± 80	194 ± 109 ^{a)}	7.0 ^{b)}
500	209 ± 81	213 ± 121 ^{a)}	6.9 ^{b)}

^{a)}Diameters of every N-NF sample measured and distribution estimated to get average diameter of mixed sample; ^{b)}Mixed sample measured with Kr physisorption.

the main nanofiber morphology stays the same during ammonolysis, but the sheet-like structure of the particles in layered perovskite Ba₅Nb₄O₁₅ nanofibers changes to smaller particles during the conversion to BaNbO₂N, which was already reported before for La₂TiO₂N.^[10,24] This proves that the nanofiber morphology is retained during the conversion of the Ba₅Nb₄O₁₅ precursor nanofibers. Similar results are known for hydrothermally grown SrTaO₂N.^[25] Additionally, the nanofiber diameter of our obtained N-NF can be adjusted by tailoring the diameter of the Ba₅Nb₄O₁₅ precursor nanofibers. The diameter of the N-NF increases from 135 up to 213 nm with an increasing amount of polymer used for the electrospinning of the Ba₅Nb₄O₁₅ precursor nanofibers.

Figure S2 of the Supporting Information displays the corresponding nanofiber diameter distributions for the investigated samples. Krypton physisorption measurements were performed to gain information about the specific Brunauer–Emmet–Teller (BET) surface area of the N-NF for photocatalytic characterization measurements. **Table 1** gives an overview of the nanofiber diameters and the BET surface areas depending on the amount of polyvinylpyrrolidone (PVP) used in the electrospinning process of the precursor Ba₅Nb₄O₁₅ nanofibers. The BET surface areas for all four N-NF samples are overall comparable with slightly increasing values upon decreasing nanofiber diameter of 6.9 up to 8.1 m² g⁻¹.

For the investigation of the bulk material, detailed X-ray diffraction (XRD) analysis was performed. XRD patterns of N-NF directly after ammonolysis are shown in **Figure 2**. No reflections belonging to the precursor nanofibers Ba₅Nb₄O₁₅ are present in all four nanofiber samples, therefore suggesting the successful conversion to phase pure BaNbO₂N. Furthermore, no reflections attributable to barium oxide are present in the XRD patterns, which is why an additional washing step was not performed, which is mostly done in other reported syntheses to remove excess BaO.^[8–12]

At careful observation, the XRD reflections of BaNbO₂N exhibit asymmetric tailing toward lower diffraction angles, which has been ascribed to possible defect formation within the perovskite lattice.^[26] However, a single-phase Rietveld refinement of BaNbO₂N (with asymmetry assumption) is not satisfactory, as can be seen in Figure S3 of the Supporting Information. Additionally, Suemoto et al. showed the emergence of Sr₂TaO₃N for SrTaO₂N—which is isostructural with BaNbO₂N—if the Sr/Ta ratio is ≥1.2.^[26] Ba₂NbO₃N was therefore included within the Rietveld refinements resulting in satisfactory quality of the data, although Rietveld refinements are still complicated due to reflection broadening and closely overlapping reflections,

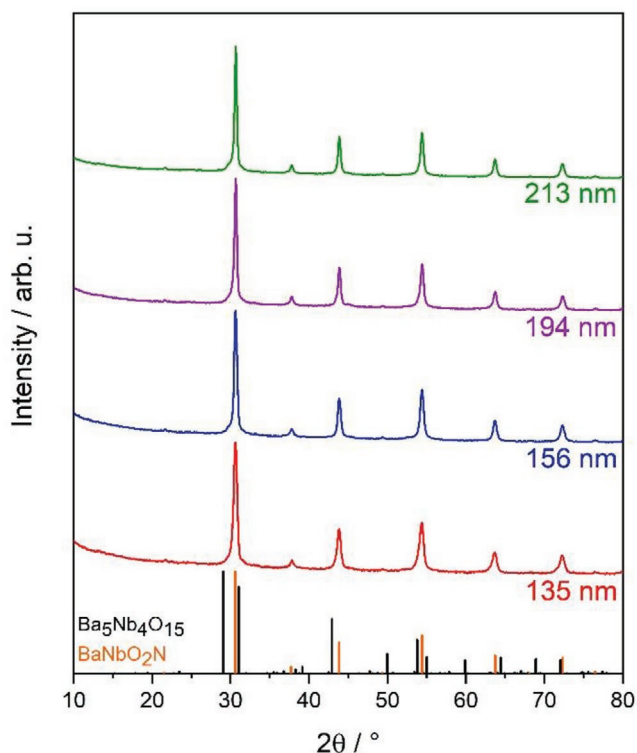


Figure 2. XRD patterns of N-NF with nanofiber diameter of 135 nm (red), 156 nm (blue), 194 nm (purple), and 213 nm (green). Calculated reference pattern of $\text{Ba}_5\text{Nb}_4\text{O}_{15}$ (black, COD 96-230-0161) and BaNbO_2N (orange, COD 01-078-1456 and Fujii et al.^[6]) are shown for comparison.

which is shown in Figure S4 of the Supporting Information. Quantitative analysis of a selected sample directly after ammonolysis in **Figure 3**—nanofibers with 156 nm diameter—shows BaNbO_2N as majority phase (77.5 wt%) and 22.6 wt% $\text{Ba}_2\text{NbO}_3\text{N}$ as secondary phase. This is a very important result, since at a first glance no by-phase can be observed in the XRD

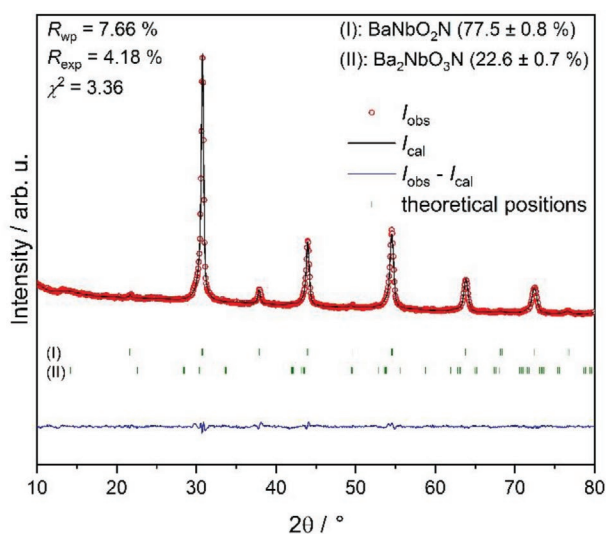


Figure 3. Rietveld refinement of N-NF with a diameter of 156 nm directly after ammonolysis.

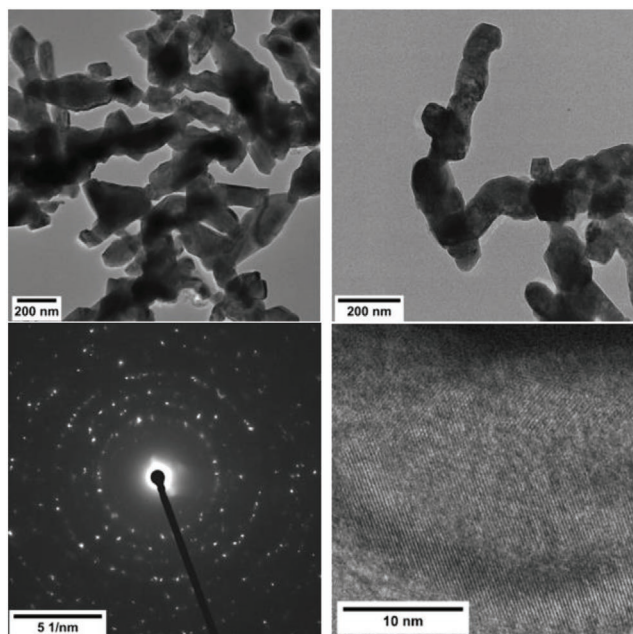


Figure 4. Transmission electron microscopy (TEM) images and SAED pattern of N-NF with 135 nm diameter.

patterns in **Figure 2**. Such detailed phase analysis shall be very important for other ammonolysis reactions and oxynitride formations as well.

Selected area electron diffraction (SAED) and visible lattice planes in **Figure 4** confirm the formation of a highly crystalline fiber sample. Due to very similar lattice planes of BaNbO_2N and $\text{Ba}_2\text{NbO}_3\text{N}$ it is not possible to assign them to one of the two oxynitrides unambiguously. Stacking faults in the BaNbO_2N – $\text{Ba}_2\text{NbO}_3\text{N}$ nanofibers, which were shown by Suemoto et al.,^[26] cannot be found.

XRD analysis of the N-NF samples stored for a few weeks shows additional reflections in the XRD pattern, which can be assigned to BaCO_3 (**Figure S5**, Supporting Information). Rietveld refinements of these samples in **Figure 5** show amounts of 4–7 wt% of BaCO_3 and additionally, similar (71–78 wt%) amounts of BaNbO_2N , whereas the amounts of $\text{Ba}_2\text{NbO}_3\text{N}$ have been decreasing (16–23 wt%) compared to samples measured directly after ammonolysis. We therefore consider it highly likely that it is indeed $\text{Ba}_2\text{NbO}_3\text{N}$ and not the main phase BaNbO_2N , which is decomposing here with time. Suemoto et al. showed the decomposition of isostructural $\text{Sr}_2\text{TaO}_3\text{N}$ toward SrCO_3 after exposure to humidity at ambient conditions,^[26] which also corroborates the presence of $\text{Ba}_2\text{NbO}_3\text{N}$ in samples here. Crystal-size sizes for BaNbO_2N in the four mixed sample batches range from 25 to 35 nm, as compared to 5–7 nm for $\text{Ba}_2\text{NbO}_3\text{N}$ and 25–28 nm for BaCO_3 and can be considered highly consistent.

The comparison of diffuse reflectance infrared Fourier transform (DRIFT) spectra of N-NF directly after the ammonolysis and after storage shows the formation of carbonate species in the samples after storage, which are not present in the samples directly after ammonolysis (**Figure S6**, Supporting Information). This further underlines the results from XRD analysis.

X-ray photoelectron spectroscopy (XPS) analysis was performed on the thinnest nanofibers stored for a few weeks

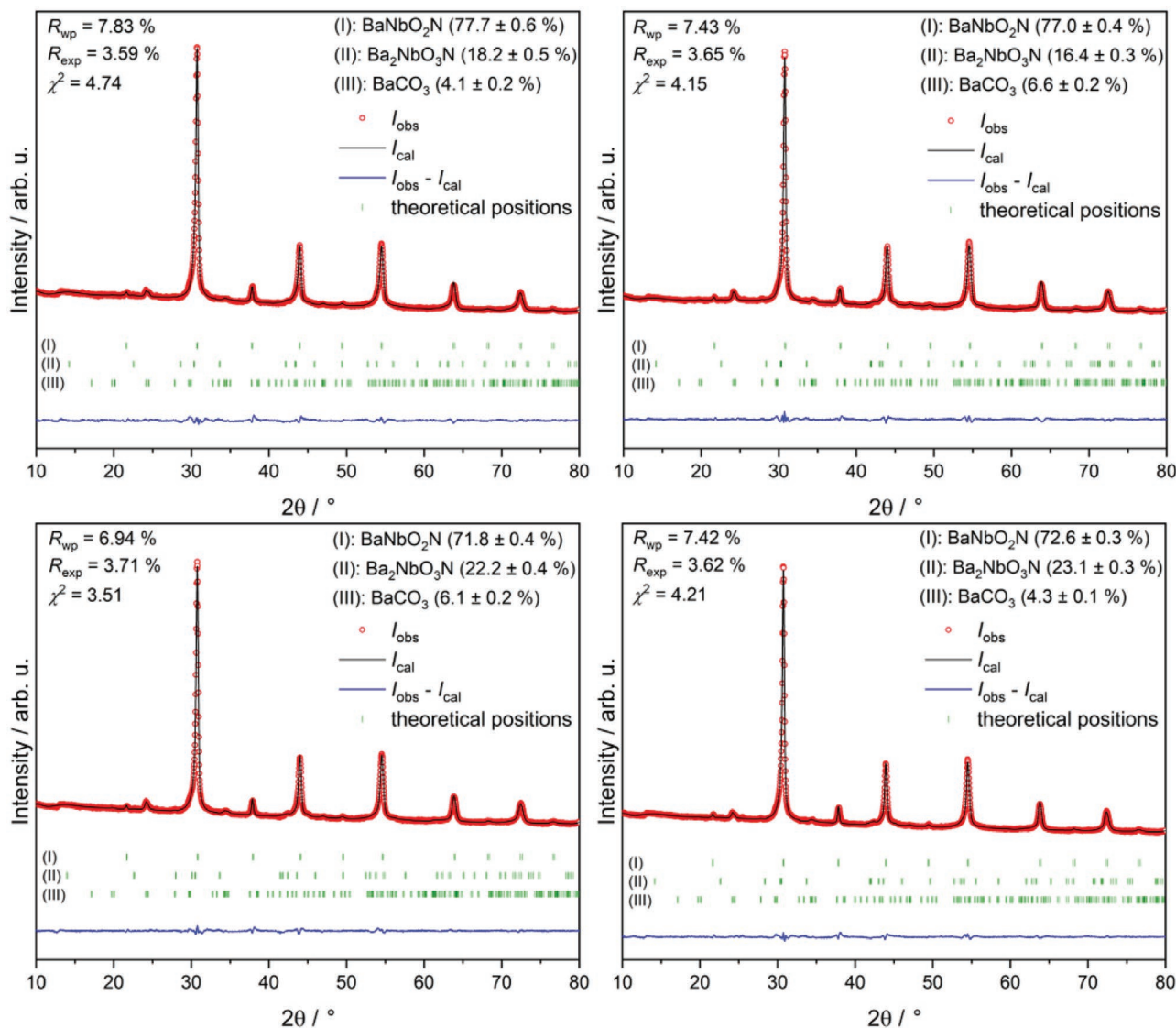


Figure 5. Rietveld refinements of all four stored N-NF samples with nanofiber diameter of (upper left) 135 nm, (upper right) 156 nm, (lower left) 194 nm, and (lower right) 213 nm.

after ammonolysis. Survey XPS data in Figure S7 of the Supporting Information show a surface elemental distribution of 13.5 at% Ba, 10.9 at% Nb, 41.5 at% O, 5.4 at% N, and 28.6 at% C. No other impurities besides the always-present adventitious carbon could be detected. Compared to the nominal stoichiometry, the surface has a slight Ba excess and a severe N deficiency and O excess, respectively.

Energy-dispersive X-ray (EDX) analysis gives Ba/Nb ratios in the same range of 1.23 to 1.26, which is highly similar to the Ba/Nb ratio as in the $\text{Ba}_5\text{Nb}_4\text{O}_{15}$ precursor nanofibers with 1.25. The determined Ba excess further underlines the result of the XRD analysis. A slight Ba excess is expected if $\text{Ba}_2\text{NbO}_3\text{N}$ is formed as by-product and no Ba is evaporated during the ammonolysis process.

Elemental analysis was performed for determination of the exact nitrogen amount in the converted nanofiber samples. The nitrogen content of all four N-NF samples stored

is in a comparable range of 3.23 to 3.39 wt%. The theoretical value of nitrogen in the samples was calculated by taking the phase composition obtained by quantitative Rietveld analysis (Figure 5) into account, leading to a theoretical value of 4.4 to 4.5 wt%, the samples showing a slight nitrogen deficiency. The nitrogen deficiency—corresponding with slight oxygen excess—can be explained by surface oxidation shown by XPS analysis (Figure 6): the Nb 3d signals are highly complex with four different components with binding energies (for Nb $3d_{5/2}$) of 206.3 eV (32.2%), 205.1 eV (64.3%), 203.3 eV (1.6%), and 202.0 eV (2.0%). The first (206.3 eV) can be ascribed to Nb(V) oxides.^[27,28]

The second peak (205.1 eV) has sometimes also been ascribed to a not specified Nb^{4+} state.^[11] However, the values in the literature reported for Nb^{4+} , i.e., niobium(IV) oxide NbO_2 are at higher binding energies than the herein measured value.^[28–31] We thus attribute this signal to BaNbO_2N , since the

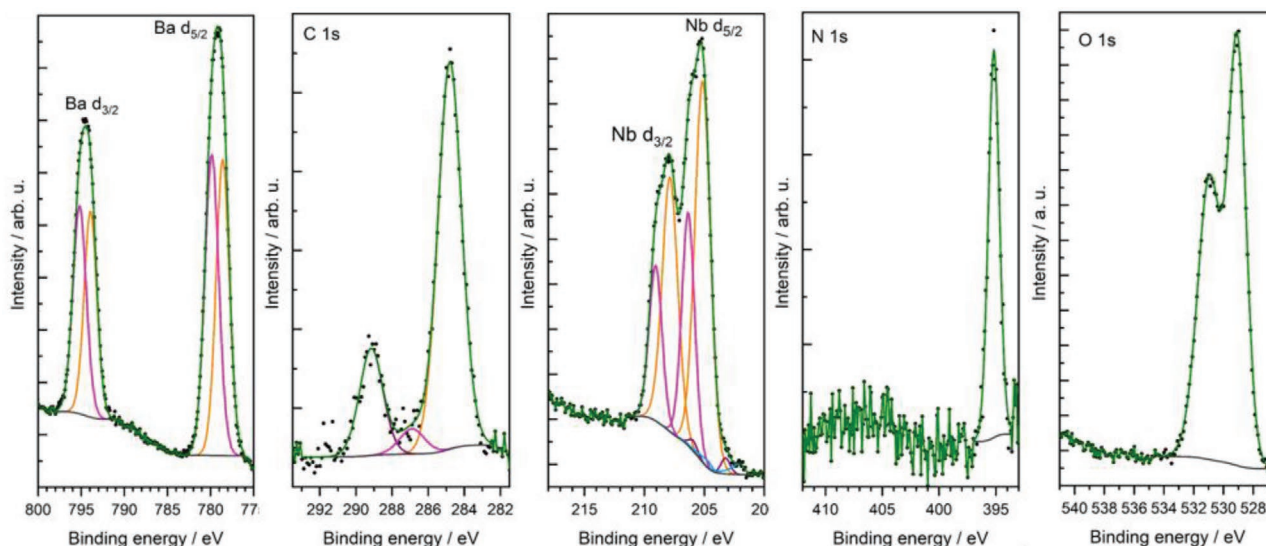


Figure 6. High-resolution XPS spectra of Ba 3d signals (left), C 1s signals (middle left), Nb 3d signals (middle), N 1s signal (middle right), and O 1s signals (right) for nanofiber sample with diameter of 135 nm after storage. Black circles indicate the measurements points, blue line the background, green line the envelope curve, and orange, pink, light blue, and purple lines the fitting curves.

measured value is highly similar to those reported for niobium oxynitride NbON.^[32–34]

The third and far smaller component (203.3 eV) can be ascribed to niobium nitride NbN,^[27,32,33,35] which seems to form in a small amount during ammonolysis. The fourth component (202.0 eV) can be assigned to elemental Nb, which is likewise formed.^[27,28,35,36] Although the oxynitride component is by far the most prevalent, the existence of a substantial Nb(V) oxide component indicates that the oxynitride is unstable and oxidized, which would also explain the N deficiency inferred from the survey spectra.

High-resolution XPS spectra of the Ba 3d region show two separate peaks for both 3d_{5/2} and 3d_{3/2} signals, the respective binding energies are 778.2 and 779.9 eV for the 3d_{5/2} signal. The first can be ascribed to mixed Ba oxides, whereas the latter is typical for BaCO₃,^[27,37] which has been observed before on Ba containing perovskites.^[37] The corresponding C 1s signal has been observed at 289.2 eV, whereas the other C 1s peaks are typical for adventitious carbon.

The N 1s spectrum consists of a single signal at 395.2 eV, which is lower than normally observed for nitrides, but highly similar to reported binding energies for niobium oxynitride NbON and BaNbO₂N.^[19,27,38]

The O 1s spectrum consists of minimum two different components but could be also fitted with up to six components. An unambiguous analysis is thus not possible as all fittings would be of good quality (not shown).

The temperature stability was further investigated by thermogravimetric analysis coupled with online mass spectrometry (TG-MS) in a temperature range of 200 to 1000 °C in synthetic air (Figure S8, Supporting Information): a slight mass loss can be observed up to 200 °C with an increase in the MS signal of H₂O ($m/z = 18$). Adsorbed water on the oxynitride surface desorbs in this temperature range. Afterward, the mass increases up to 600 °C, which can be assigned to the oxidation of the barium niobium oxynitride, followed by a stepwise decrease

of the mass up to a temperature of 850 °C. A peak in the MS signal assigned to CO₂ ($m/z = 44$) is detected in the temperature range of 500 up to 800 °C, which can be assigned to the decomposition of the formed BaCO₃. The stepwise decrease of the mass is due to the release of nitrogen. This could not be detected via MS since synthetic air was used as carrier gas. The curve progression is in good agreement with TG-MS curves of SrNbO₂N measured in an atmosphere with 20% oxygen.^[39]

Optical properties were analyzed by diffuse reflectance measurements, which were converted to Kubelka–Munk spectra and Tauc plots for bandgap estimation (Figure 7). The conversion of Ba₅Nb₄O₁₅ nanofibers to BaNbO₂N–Ba₂NbO₃N nanofibers leads to a visible light absorption compared to UV light-only absorption for the precursor nanofibers. This corresponds to a decrease of the indirect bandgap from 3.9 eV for Ba₅Nb₄O₁₅ to ≈1.8 eV for the converted nanofiber composite samples. Since the resulting material consists of a composite, the term bandgap is not fully correct here, but the shift in the absorption edge by more than 2 eV is very prominent. All four samples exhibit absorption edges at 1.7 to 1.8 eV, which is in correspondence to the reported literature.^[7–11,13,16,18,14] The first derivation of the reflectance spectra in Figure S9 of the Supporting Information shows that the main absorption edge shows only one maximum, therefore only of BaNbO₂N. A clear attribution of the very small absorption maxima at 495 nm cannot be given. Furthermore, Cen et al. performed theoretical calculations on the electronic structure of Ba₂NbO₃N and showed that this Ruddlesden–Popper perovskite is a direct semiconductor material with a theoretical bandgap of 2.0 to 2.13 eV with decreasing bandgap going from one layered to three layered Ba₂NbO₃N.^[40] Therefore direct bandgaps of the samples were also estimated (Figure 7). Absorption edges are all in the range of 2.6 to 2.8 eV, compared to 4.3 eV for the precursor nanofibers. This is slightly higher than the value obtained from theoretical calculations of the Ruddlesden–Popper perovskite Ba₂NbO₃N, which is also the case for the indirect bandgap of BaNbO₂N, which has been

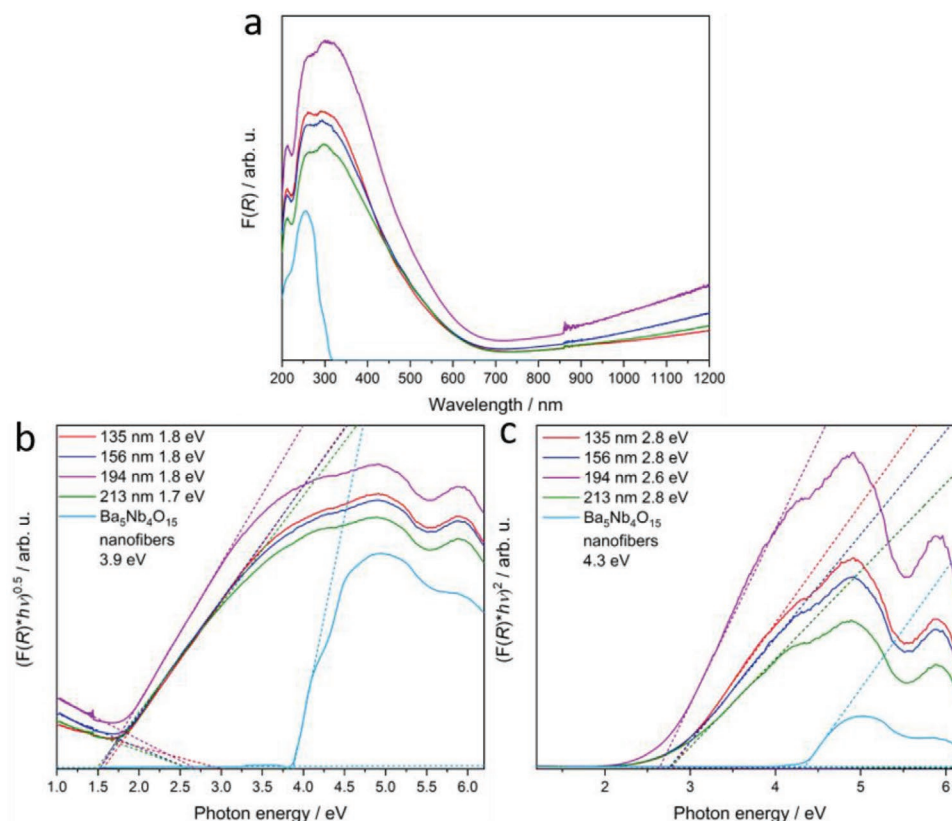


Figure 7. a) Kubelka–Munk UV–vis spectra, b) indirect Tauc plots, and c) direct Tauc plot of BaNbO_2N – $\text{Ba}_2\text{NbO}_3\text{N}$ nanofiber batches with 135 nm (red), 156 nm (dark blue), 194 nm (purple), and 213 nm (green) and of $\text{Ba}_5\text{Nb}_4\text{O}_{15}$ nanofibers (light blue) for comparison.

calculated to be 1.4 to 1.6 eV.^[41] Resulting from this, it can be concluded that the diffuse reflectance analysis confirms the presence of BaNbO_2N – $\text{Ba}_2\text{NbO}_3\text{N}$ composite nanofibers.

2.2. Photocatalytic Hydrogen and Oxygen Evolution Results and Post-Photocatalytic Characterization

Photocatalytic hydrogen and oxygen evolution experiments were performed with BaNbO_2N – $\text{Ba}_2\text{NbO}_3\text{N}$ nanofibers of different diameters after storage, to investigate their photocatalytic activity and the potential influence of the nanofiber diameter. A doped mercury lamp in a borosilicate housing was used, which cuts off all light intensity smaller than 300 nm (Figure S10, Supporting Information).

For the hydrogen evolution reaction, the nanofiber samples were dispersed in a mixture of water and methanol as sacrificial agent, the hydrogen evolution rate was measured with and without cocatalyst. The optimum amount of Pt cocatalyst was estimated on one exemplary sample by a stepwise photodeposition of Pt until no further increase in the hydrogen evolution rate could be detected, and was determined to be 0.5 wt% (Figure S11, Supporting Information). This amount was then recalculated respective to the absolute surface area, resulting in $3.66 \mu\text{mol m}^{-2}$ Pt; this amount was used for the further hydrogen evolution measurements of all samples. The surface specific loading with cocatalyst was shown to be very important

for the comparison of photocatalytic activities of nanostructured materials.^[21,42]

All nanofiber samples are able to produce hydrogen without the addition of cocatalyst, as can be seen in the first 3 h of the measurement (Figure 8). The hydrogen evolution rate without addition of a cocatalyst is 0.8 to $1.0 \mu\text{mol h}^{-1}$ for all four nanofiber samples and is therefore comparable. After Pt decoration, the fiber samples with the highest and smallest diameter and surface area show the same rate with $2.8 \mu\text{mol h}^{-1}$ (Figure 8 left).

To exclude the influence of surface area and investigate the activity dependence solely on fiber diameter, Figure 8 right shows the hydrogen evolution curves, normalized on absolute surface area to compensate for the influence of different numbers of active sites due to differences in surface area. This conversion was recently reviewed as being very important for nanostructured and porous materials with high specific surface area, for the evaluation of the real influence of specific surface area enhancement.^[43] Here, since the influence of the fiber diameter shall be discussed, the absolute surface area is taken into account by this normalization.

The evolution rates without cocatalyst are still in the same range for all samples. The hydrogen evolution rate increases two- to threefold after the addition of Pt. The most pronounced increase to $3.1 \mu\text{mol h}^{-1} \text{m}^{-2}$ is obtained for the nanofiber sample with the largest nanofiber diameter of 213 nm, followed by the sample with the smallest diameter with $2.6 \mu\text{mol h}^{-1} \text{m}^{-2}$.

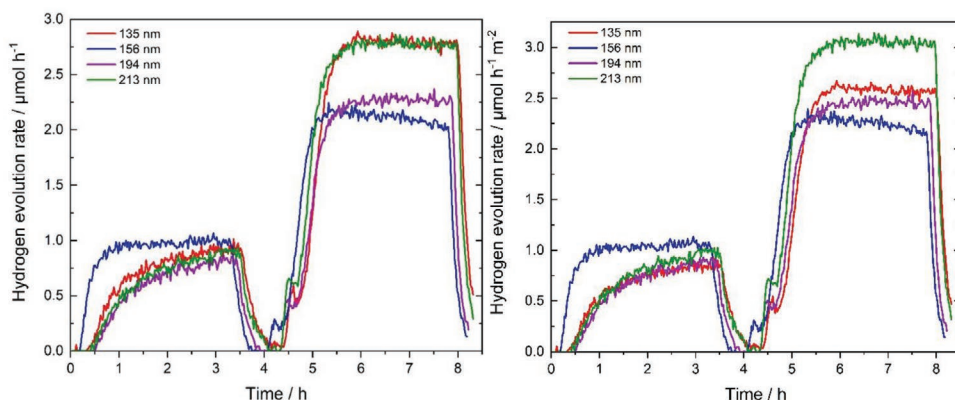


Figure 8. Hydrogen evolution curves of BaNbO₂N–Ba₂NbO₃N after storage with diameters of 135 nm (red), 156 nm (blue), 194 nm (purple), and 213 nm (green) non-normalized (left) and normalized on absolute surface area (right), without cocatalyst in the first 3 h and with Pt as cocatalyst in the second 3 h. Lamp was turned off after 3.25 to 3.5 h and on again after 4.0 to 4.25 h for cocatalyst addition and off after 7.75 to 8.0 h.

This trend is now different compared to the non-normalized rate, since by using the same catalyst mass a different surface area is in contact with the electrolyte. This indicates that surface area and diameter, as expected, both have an influence on the activity. The thickest oxynitride nanofibers show the highest activity, likely due to structural or morphological differences as we reported before for diameter-adjusted Ba₅Ta₄O₁₅ nanofibers.^[21] The nitrogen evolution was also tracked in these experiments to investigate the degradation of samples and shows only maximum values of 0 to 0.4 μmol h⁻¹ (not shown).

Characterization of the samples after the hydrogen evolution reaction shows a less pronounced tailing of the reflections of BaNbO₂N in the XRD patterns, no BaCO₃ reflections are visible anymore (Figure S12, Supporting Information). Single-Rietveld refinements of BaNbO₂N (with asymmetric assumption) are in all four cases satisfying (Figure S13, Supporting Information), which confirm that indeed Ba₂NbO₃N decomposes and not BaNbO₂N. The Kubelka–Munk spectra show comparable absorption edges for all samples, demonstrating that BaNbO₂N is not decomposed during the hydrogen evolution reaction (Figure S12, Supporting Information). This can be further underlined by elemental analysis after hydrogen evolution reaction with comparable values of 3.2 to 3.3 wt% nitrogen and only the small amounts of nitrogen gas, which are detected during photocatalytic reaction. Exemplary SEM image of nanofibers with diameter of 213 nm after hydrogen evolution reaction (Figure S14, Supporting Information) shows small nanofiber pieces, which can be explained by the sample preparation (ultrasonication) and stirring during the reaction time.

Additionally, the activity of the composite samples regarding oxygen evolution reaction was tested. Since it was already reported that BaNbO₂N is not able to produce oxygen without the addition of a cocatalyst,^[7,14] CoO_x was deposited as cocatalyst via an impregnation method followed by subsequent annealing in ammonia and air following literature.^[44] However, XRD pattern after the deposition shows additional reflections, which can be assigned to CoNbO₄ and hexagonal Ba₄Nb₂O₉ (Figure 9). The appearance of additional reflections after the deposition process was already reported before for BaTaO₂N, however has not been assigned to cobalt containing phases before, but to amorphous Co species instead.^[45]

These CoNbO₄-decorated samples were then dispersed in water together with La₂O₃ as pH buffer (pH ≈ 8) for the oxygen evolution reaction, and the oxygen evolution was measured with the same setup as was used for the hydrogen evolution. Cobalt loadings of 1 or 2 wt% were tested on one sample (156 nm diameter) in water with silver nitrate as sacrificial agent (Figure S11, Supporting Information). Co loading of 2 wt% resulted in higher oxygen evolution amounts when the first 2 h were considered, thus it was used as loading for all

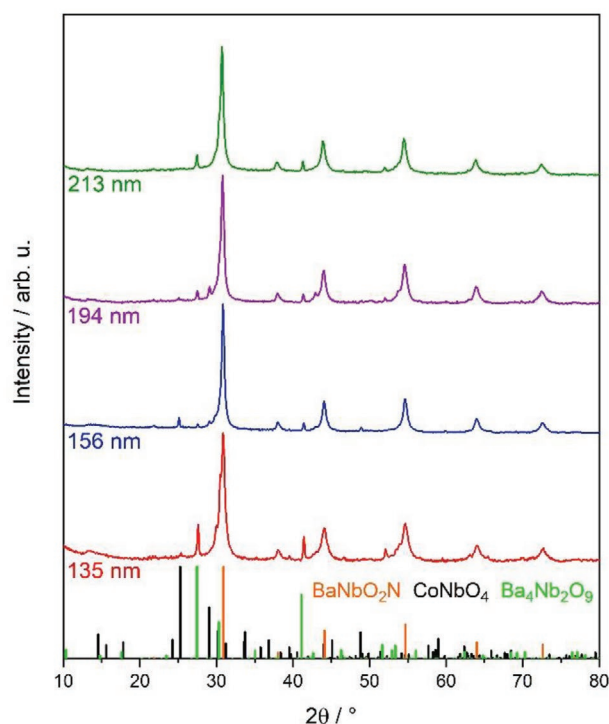


Figure 9. XRD pattern after CoNbO₄ deposition on BaNbO₂N–Ba₂NbO₃N nanofiber batches with 135 nm (red), 156 nm (blue), 194 nm (purple), and 213 nm (green) diameter. Calculated reference pattern of BaNbO₂N (orange, COD 01-078-1456 and Fujii et al.^[6]), CoNbO₄ (black, ICDS 98-001-6377), and Ba₄Nb₂O₉ (light green, COD 96-400-1053) are shown for comparison.

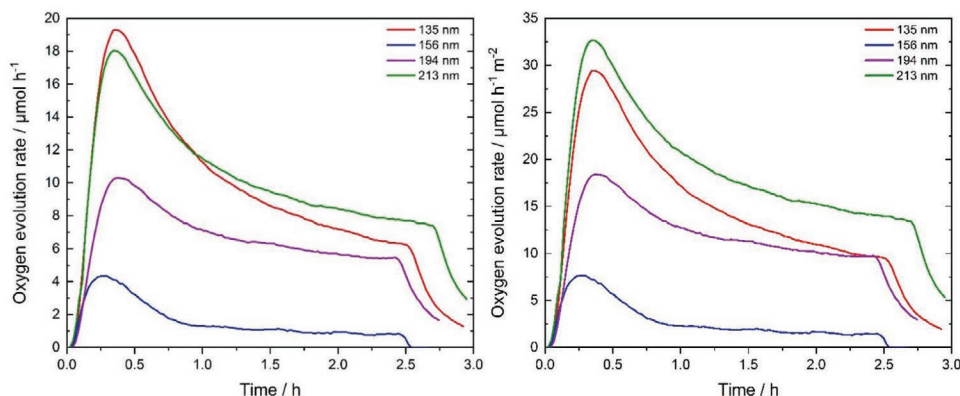


Figure 10. Oxygen evolution curves of CoNbO₄ deposited BaNbO₂N–Ba₂NbO₃N samples after storage with diameters of 135 nm (red), 156 nm (blue), 194 nm (purple), and 213 nm (green) non-normalized (left) and normalized on absolute surface area (right). Lamp turned off after 2.5 to 2.75 h.

nanofiber samples. Without the addition of silver nitrate as sacrificial agent, only small amounts of 0 to 0.4 μmol oxygen and 0.3 μmol to 0.7 μmol nitrogen were detected for all samples (not shown). After the addition of silver nitrate as sacrificial agent, a pronounced increase in oxygen evolution could be observed. **Figure 10** shows the oxygen evolution after the addition of silver nitrate for all four CoNbO₄ decorated nanofiber composite samples: all samples produce oxygen. The activity trends regarding the nanofiber diameter is comparable to the results of the hydrogen evolution reaction (Figure 8 left). The nanofibers with lowest and highest diameter and surface area show the highest activity with 22.7 and 23.0 μmol oxygen evolution (Figure 10 left). After normalization to absolute surface area (Figure 10 right), the nanofibers with the highest fiber diameter clearly exhibit the highest activity with 32.7 μmol h⁻¹ m⁻² in maximum, followed by the fibers with the smallest diameter with 29.5 μmol h⁻¹ m⁻². Nanofibers with 194 nm exhibit a maximum of 18.4 μmol h⁻¹ m⁻² and fibers with 156 nm in diameter show the lowest rate with 7.7 μmol h⁻¹ m⁻² in maximum. Nitrogen evolution rates after addition of silver nitrate were comparably negligible as before, showing that the oxynitride samples are stable against decomposition (not shown). Due to the fact, that a comparison of the maxima in the oxygen evolution rates is not that precise, the absolute amount of oxygen in the first 2 h after addition of silver nitrate was calculated by integration. **Table 2** summarizes these values and the

Table 2. Hydrogen evolution rates and amount of oxygen evolved in oxygen evolution reaction depending on the nanofiber diameter, non-normalized and normalized on absolute surface area.

Nanofiber diameter [nm]	Hydrogen evolution rate ^{a)} [μmol h ⁻¹]	Hydrogen evolution rate ^{a)} [μmol h ⁻¹ m ⁻²]	Oxygen evolution ^{b)} [μmol]	Oxygen evolution ^{b)} [μmol m ⁻²]
135	0.9 ^{c)} /2.8 ^{d)}	0.8 ^{c)} /2.6 ^{d)}	22.7 ^{b)}	34.6 ^{b)}
156	1.0 ^{c)} /2.0 ^{d)}	1.1 ^{c)} /2.2 ^{d)}	3.7 ^{b)}	6.5 ^{b)}
194	0.8 ^{c)} /2.3 ^{d)}	0.9 ^{c)} /2.4 ^{d)}	14.3 ^{b)}	25.3 ^{b)}
213	0.9 ^{c)} /2.8 ^{d)}	1.0 ^{c)} /3.1 ^{d)}	23.0 ^{b)}	41.3 ^{b)}

^{a)}Steady-state value; ^{b)}Amount of oxygen in the first 2 h after AgNO₃ addition, calculated by integration; ^{c)}Evolution rate without cocatalyst deposited; ^{d)}Evolution rate with 3.66 μmol m⁻² Pt deposited.

evolution rates of the hydrogen evolution reaction depending on the nanofiber diameter for the non-normalized and to absolute surface area normalized data.

Sample characterization after the oxygen evolution reaction via XRD characterization is not shown, due to the high amount of La₂O₃ added as buffer, which severely compromises the analysis of XRD patterns. Moreover, silver deposited during the oxygen evolution reaction precludes diffuse reflectance measurements.

Comparing these results with regards to the influence of nanofiber diameters with the diameter-dependent study of photocatalytic water splitting on Ba₅Ta₄O₁₅ nanofibers, the trend in the activities is different: after optimization of the cocatalyst loading, a 161 nm as optimum diameter was reported, followed by comparable values for thicker nanofibers with 228 nm and smallest fiber diameter with 109 nm.^[21] Comparable to this, the activities in the present study first decrease with decreasing fiber diameters but then increase again for fibers with the smallest diameter of 135 nm. One reason for the higher activities of the thinnest and the thickest oxynitride nanofiber composites—compared to fibers of the layered perovskite—could be the competitive effects of crystallinity and anion deficiency in the nitridation process of BaNbO₂N with different micrometer sizes postulated by Yamada et al.^[10]

Hydrogen and oxygen evolution reactions with a 300 W Xe lamp equipped with an AM1.5G filter on the most active nanofiber sample with 213 nm with cocatalyst surprisingly did not show any gas evolution, in contrast to reported visible light activity of BaNbO₂N.^[7-9,13,19] This will be investigated in the future.

Finally, overall water splitting activity was investigated on the most active sample (213 nm diameter). For this, Pt was first photodeposited on the sample and afterward cobalt was deposited via the impregnation method. The gas evolution is shown in Figure S15 of the Supporting Information. Only very small amounts of gas could be detected. The decomposition process of the sample, forming N₂ seems to be preferred. Comparing hydrogen and oxygen evolution values, slightly more oxygen is evolved, although a 2:1 ratio of hydrogen to oxygen is expected in overall water splitting. This in correspondence to the significant lower hydrogen evolution activity compared to the oxygen evolution activity with cocatalyst

deposited. Instead of the reduction of protons, it seems that the photocatalyst itself is decomposed in pure water. XRD pattern after overall water splitting experiment in Figure S16 of the Supporting Information shows reflections belonging to BaNbO₂N with a reduced tailing, which confirms the results of the decomposition of Ba₂NbO₃N from XRD patterns after hydrogen evolution reaction. Furthermore, the additional reflections after CoO_x deposition are not visible anymore, indicating, that these phases are not stable under the overall water splitting conditions.

3. Conclusion

The conversion of electrospun Ba₅Nb₄O₁₅ nanofibers with adjusted diameters via an ammonolysis reaction led to the formation of oxynitride nanofibers with retained nanofiber morphology. Moreover, the nanofiber diameter was adjusted in a range of 135 up to 213 nm. Most importantly, only very detailed material characterization revealed that the resulting oxynitride is actually a novel BaNbO₂N–Ba₂NbO₃N composite, and not sole BaNbO₂N. A diameter-dependent photocatalytic hydrogen and oxygen evolution activity could be shown with an optimum nanofiber diameter of 213 nm. Pt and CoNbO₄ cocatalyst deposited fibers with optimum diameter exhibited a performance of 3.1 μmol h⁻¹ m⁻² in hydrogen evolution and 41.3 μmol m⁻² in oxygen evolution reaction. The influence of Ba₂NbO₃N on photocatalytic activity has to be investigated in the future. Nevertheless, this novel approach of nanostructuring semiconductors for ammonolysis reactions could be a way to synthesize other photocatalytically active oxynitride semiconductors with beneficial nanostructures.

4. Experimental Section

Chemicals: Barium(II) ethylhexanoate (98%, Sigma-Aldrich), niobium(V) ethoxide (99.9%, abcr, used as a 0.24 M solution in absolute ethanol (extra dry, 99.5%, AcrosOrganics), PVP (MW = 1 300 000, Alfa Aesar), tetrahydrofuran (technical grade, VWR), lanthanum oxide (99.9%, Strategic Elements), hydrogen hexachloroplatinate(IV) hydrate (99.995%, Carl Roth), cobalt(II) nitrate hexahydrate (99%, abcr), silver nitrate (99.8–100.5%, VWR), and methanol (99.9%, Fisher chemical). Lanthanum oxide was heated to 600 °C for 10 h before usage. All other chemicals were used as received.

Synthesis of Ba₅Nb₄O₁₅ Nanofibers as Precursors for BaNbO₂N Nanofibers: Ba₅Nb₄O₁₅ nanofibers were synthesized according to the route reported by Hildebrandt et al., and nanofiber diameters were adjusted as shown by Bloesser et al.^[20,21] For one batch of Ba₅Nb₄O₁₅ nanofibers, 890 mg of barium(2-ethylhexanoate) was dissolved in 3 mL of THF and 7 mL of a 0.24 Nb(OEt)₅ solution in absolute ethanol was added. Then, 200 to 500 mg of PVP were added and the solution was stirred until a clear spinning solution was obtained. The solution was filled in a syringe equipped with a cannula with an inner diameter of 0.8 mm and a flat-cut tip, and placed in a syringe pump for the electrospinning process in a home-made electrospinning chamber. The humidity in the chamber was set to 30%, the distance between the tip of the cannula and the rotating drum collector to 15 cm, a potential of +18 kV at the cannula and –2 kV at the collector was applied, and the solution was pumped with a rate of 0.3 mL min⁻¹. The obtained fibers were calcined at 1173 K for 10 h (heating rate of 5 K min⁻¹) in a muffle furnace in air for removal of the spinning polymer and crystallization of Ba₅Nb₄O₁₅.

Synthesis of BaNbO₂N Nanofibers: The BaNbO₂N nanofibers were prepared by an ammonolysis reaction of the synthesized Ba₅Nb₄O₁₅ precursor nanofibers. Ba₅Nb₄O₁₅ nanofibers were placed in a quartz boat and were annealed in an NH₃ flow of 60 mL min⁻¹ at 1273 K for 20 h in a tube furnace. The heating was performed in an Ar flow with a heating rate of 10 K min⁻¹ and the sample was also cooled down in Ar flow to room temperature. To obtain enough material for the photocatalytic characterization of the BaNbO₂N nanofibers, two to three charges were mixed after thorough characterization.

Characterization Methods: SEM images were recorded with a Zeiss LEO 1530. All samples were sputtered with 1 to 2 nm Pt using a Cressington Sputter Coater 208 HR. An acceleration voltage of 3 kV was applied with an aperture set to 30 μm. For EDX analysis an UltraDry-EDX detector (ThermoFisher Scientific NS7) was used, the voltage was set to 20 kV, and the aperture to 60 μm. For each sample, the Ba/Nb ratio was averaged from measurements of several areas.

TEM images were recorded with a JEOL JEM-2200FS EFTEM equipped with Schottky FEG and In-Column Omega Energyfilter from JEOL operated at 200 kV. Prior the measurement, 1 to 2 mg of the sample were suspended in 1 mL of ethanol (AcrosOrganics, extra dry, 99.5%). Then, 4 μL of the suspension was dropped on a carbon film coated Cu TEM grid (200 Mesh). TEM images were processed using ImageJ.

XRD was measured on an Empyrean diffractometer (Malvern PANalytical) with a PixCel 1D detector using Cu Kα radiation. Rietveld refinements were performed using the program Fullprof with a Thompson-Cox-Hastings pseudo-Voigt function with asymmetry as profile function and a Chebychev polynomial for background approximation.^[46] Instrumental broadening was determined with a LaB₆ standard (NIST SRM660c). Due to the similar mass attenuation coefficients and the small crystallite sizes microabsorption was neglected. Information about the crystal structure for refinements were taken from Fujii et al. for BaNbO₂N,^[6] Clarke et al. for Ba₂NbO₃N (adjusted accordingly),^[47] and Antao and Hassan for BaCO₃.^[48] Theoretical diffraction patterns were calculated using Diamond (Crystal Impact). Information about the crystal structure were taken from Cernik et al. for Ba₅Nb₄O₁₅,^[49] Lehmann and Müller-Buschbaum for CoNbO₄,^[50] and Ling et al. for h-Ba₄Nb₂O₉.^[51]

DRIFT spectra were collected using a Bruker Alpha II with interchangeable measurement modules.

XPS was measured on a VersaProbe III Scanning XPS Microprobe from Physical Electronics PHI using monochromatic Al Kα radiation and a beam diameter of 100 μm. Survey spectra were recorded with a pass energy of 224 eV and a step size of 0.8 eV, whereas high-resolution spectra were recorded with a pass energy of 26 eV and a step size of 0.1 eV; integration time was 50 ms in both cases. The sample was flooded with slow-moving electrons and argon ions during measurement to prevent surface charging. The sample was not argon sputter cleaned prior to measurement to prevent reduction of the surface. Data analysis was performed using CasaXPS; Shirley backgrounds and Gaussian–Lorentzian (GL30) peak-shapes were used for ionic components and asymmetric LA(1.2,5,12) peak-shapes for metallic Nb. For charge correction, the C 1s signal was set to 284.8 eV.

TG analysis in synthetic air was performed with a Netzsch Jupiter STA 449C thermobalance, which was additionally coupled with a Netzsch Aeolos QMS 403C quadrupole MS for recording gaseous compounds, i.e., H₂O (18), N₂ (28), and CO₂ (44).

Krypton physisorption measurements at 77 K were recorded with ASiQ-MP-MP-AG setup (Anton Paar QuantaTec, Boynton Beach, USA). Prior to the measurement the samples were degassed for 3 h at 200 °C in vacuum. The data analysis was done using the BET model via software ASiQwin (Anton Paar QuantaTec, Boynton Beach, USA). The saturation pressure *p*₀ was kept constant at 2.63 Torr.

Elemental analysis (C, H, N, S) was measured with a Unicube from Elementar with sulfanilamide as the standard. Precise quantities of samples between 2 and 4 mg were placed in a tin boat and sealed prior to the measurement. To ensure the complete combustion of the samples, the combustion tube was heated up to 1143 °C in O₂/Ar

atmosphere. The detection of completely oxidized gas species was done via thermal conductivity system.

A PerkinElmer Lambda 750 UV/vis/NIR spectrometer, equipped with a Praying-Mantis mirror unit from Harrick was used to record the diffuse reflectance with step size of 1 nm. A spectralon pellet was used as white standard. The spectra were converted into absorption spectra using Kubelka–Munk function; bandgaps were estimated using Tauc plots.

Lamp spectra were measured with a Flame spectrometer from Ocean Insight.

Photocatalytic Hydrogen Evolution Experiments: Ultrapure water was used for all hydrogen evolution reactions. A dispersion of 132 mg photocatalyst in 550 mL water and 50 mL methanol was prepared with ultrasonication for 15 min. The dispersion was filled into a homemade double-walled inner-irradiation glass reactor with a borosilicate housing for the lamp and was stirred with 200 rpm. A 700 W Z4 doped Hg mid-pressure lamp (Peschl UV-Consulting) set to 500 W was used, the lamp spectra are shown in Figure S10 of the Supporting Information. The temperature was set to 10 °C with a thermostat (LAUDA RP845) and the whole system was flushed with 100 mL min⁻¹ Ar 5.0 using a Bronkhorst mass flow controller for several hours to remove residual air. The gas evolution was detected online using a mass spectrometer (Hiden HPR-20 Q/C). During the experiment oxygen, hydrogen, nitrogen, and carbon dioxide were detected. To find the optimum in Pt cocatalyst loading different amounts of Pt were in situ photodeposited on one exemplary nanofiber sample by a stepwise addition of an aqueous solution of H₂PtCl₆ through a rubber sealing. After 2.5 h without any Pt codeposited, Pt loading was adjusted until the detected hydrogen evolution rate did not improve further by shortly switching off the lamp and adding a defined amount of Pt to the dispersion and turning the lamp on again. Every photodeposition step took around 1 h. The optimum Pt loading was then used for all other hydrogen evolution reactions and was adjusted, depending on the surface area of the used nanofiber sample. For the measurements of the nanofiber samples with varying diameter, the gas evolution was measured for ≈3 h to investigate the activity of the nanofiber samples without any cocatalyst deposited. Afterward the lamp was shortly switched off to add an aqueous solution of H₂PtCl₆ through a rubber sealing. The sedimented samples were centrifuged and dried at 80 °C.

Hydrogen evolution reaction with 300 W solar simulator using a Xe lamp (Quantum Design) equipped with an AM1.5G filter was conducted on the most active sample in a top-irradiated reaction vessel. Measurements were performed at 20 °C, the system was also flushed with Ar before measurement. For the measurement 68 mg of the photocatalyst was dispersed in a mixture of 135 mL water and 15 mL methanol. Gas evolution was also detected online with MS.

Deposition of Cobalt-Based Cocatalyst: The deposition was performed via an impregnation method reported by Zhang et al.^[39] An appropriate amount aqueous solution of Co(NO₃)₂·6H₂O (490 mg L⁻¹) was added to the synthesized nanofiber sample and the water was then evaporated at 100 °C under stirring. The obtained solid was placed in a quartz boat, was annealed in a NH₃ flow (200 mL min⁻¹) at 973 K (heating rate 10 K min⁻¹) for 1 h and was cooled down in an Ar flow in a tube furnace. The sample was afterward heated for 1 h at 473 K in air in a muffle furnace.

Photocatalytic Oxygen Evolution Experiments: Ultrapure water was used for all oxygen evolution reactions (cleaned with a pure water system of VWR (A series), total organic carbon (TOC) = 2 ppb). A dispersion of 80 mg of the CoO_x deposited photocatalyst and 160 mg La₂O₃ as pH buffer in 600 mL water was prepared with an ultrasonication step for 15 min. The dispersion was filled into the same reactor, conditions and lamp kept the same as for the hydrogen evolution reaction (details see above). Oxygen evolution rate in first hours was detected without addition of sacrificial agent. Then the lamp was shortly switched off and 3 M AgNO₃ solution was added through a rubber sealing to reach a concentration of 0.01 M. After all gases evolution rates reached zero again, the lamp was switched on again and the gas evolution was detected for further 2.5 h. As only a negligible amount of gases was formed without AgNO₃, only the gas evolution curves after the addition of AgNO₃ are shown and time was set to zero, when gas evolution reached 0 after AgNO₃ addition.

Oxygen evolution reaction was performed with Xe-lamp on the most active sample (65 mg) with the same conditions as already mentioned in the hydrogen evolution part, but instead of methanol silver nitrate was used as sacrificial agent (10 × 10⁻³ M) and La₂O₃ (130 mg) was added as pH buffer.

Overall Water Splitting Experiment: Ultrapure water (TOC = 2 ppb) was used for Pt photodeposition and overall water splitting experiment. Overall water splitting was tested on the most active sample in hydrogen and oxygen evolution reactions. First 3.66 μmol m⁻² Pt was photodeposited on 136 mg of the sample as described above with photodeposition time of 1 h. After this, the sample was directly evaporated to dryness, washed thoroughly with water, and dried. Then CoO_x was deposited via impregnation method. For overall water splitting, 96 mg of the Pt-CoO_x deposited nanofiber sample was immersed in 600 mL water with 15 min ultrasonication and filled in the same reactor as for hydrogen and oxygen evolution reaction. Reaction conditions and used lamp were also the same. The system was flushed with Ar overnight to remove any residual air. The gas evolution was then detected for 3 h. Gas evolution in the first 15 min can be attributed to small contaminations. Lamp was turned on after gas evolution rate was zero again after 20 min and measurement was performed for 3 h.

Supporting Information

Supporting Information is available from the Wiley Online Library or from the author.

Acknowledgements

The authors thank Christopher Simon for TEM measurements and Lena Geiling (all University of Bayreuth, Germany) for TG-MS measurements. Furthermore, the authors thank the KeyLab Device Engineering at the Bavarian Polymer Institute, University Bayreuth for use of the XPS. Additionally, the authors thank the BPI KeyLab Electron and Optical Microscopy for use of the Zeiss Leo 1530 and JEOL JEM-2200FS.

Open access funding enabled and organized by Projekt DEAL.

Conflict of Interest

The authors declare no conflict of interest.

Data Availability Statement

Research data are not shared.

Keywords

ammonolysis, electrospinning, nanofibers, oxynitride, photocatalysis

Received: June 9, 2021

Revised: June 22, 2021

Published online: July 15, 2021

[1] K. Maeda, M. Higashi, B. Siritanaratkul, R. Abe, K. Domen, *J. Am. Chem. Soc.* **2011**, *133*, 12334.

[2] A. Kasahara, K. Nukumizu, T. Takata, J. N. Kondo, M. Hara, H. Kobayashi, K. Domen, *J. Phys. Chem. B* **2003**, *107*, 791.

[3] J. Xu, C. Pan, T. Takata, K. Domen, *Chem. Commun.* **2015**, *51*, 7191.

[4] M. Higashi, K. Domen, R. Abe, *J. Am. Chem. Soc.* **2013**, *135*, 10238.

- [5] F. Pors, R. Marchand, Y. Laurent, P. Bacher, G. Roullet, *Mater. Res. Bull.* **1988**, 23, 1447.
- [6] K. Fujii, K. Shimada, M. Yashima, *J. Ceram. Soc. Jpn.* **2017**, 125, 808.
- [7] F. Oehler, S. G. Ebbinghaus, *Solid State Science*, Elsevier Masson SAS, Amsterdam **2016**, pp. 43–48.
- [8] M. Hojamberdiev, E. Zahedi, E. Nurlaela, K. Kawashima, K. Yubuta, M. Nakayama, H. Wagata, T. Minegishi, K. Domen, K. Teshima, *J. Mater. Chem. A* **2016**, 4, 12807.
- [9] T. Hisatomi, C. Katayama, Y. Moriya, T. Minegishi, M. Katayama, H. Nishiyama, T. Yamada, K. Domen, *Energy Environ. Sci.* **2013**, 6, 3595.
- [10] T. Yamada, Y. Murata, S. Suzuki, H. Wagata, S. Oishi, K. Teshima, *J. Phys. Chem. C* **2018**, 122, 8037.
- [11] J. Seo, T. Hisatomi, M. Nakabayashi, N. Shibata, T. Minegishi, M. Katayama, K. Domen, *Adv. Energy Mater.* **2018**, 8, 1800094.
- [12] J. Seo, M. Nakabayashi, T. Hisatomi, N. Shibata, T. Minegishi, M. Katayama, K. Domen, *J. Mater. Chem. A* **2019**, 7, 493.
- [13] T. Hisatomi, C. Katayama, K. Teramura, T. Takata, Y. Moriya, T. Minegishi, M. Katayama, H. Nishiyama, T. Yamada, K. Domen, *ChemSusChem* **2014**, 7, 2016.
- [14] B. Siritanaratkul, K. Maeda, T. Hisatomi, K. Domen, *ChemSusChem* **2011**, 4, 74.
- [15] Y. Il Kim, E. Lee, *J. Ceram. Soc. Jpn.* **2011**, 119, 371.
- [16] Y. Il Kim, P. M. Woodward, K. Z. Baba-Kishi, C. W. Tai, *Chem. Mater.* **2004**, 16, 1267.
- [17] J. Odahara, A. Miura, N. C. Rosero-Navarro, K. Tadanaga, *Inorg. Chem.* **2018**, 57, 24.
- [18] J. Seo, Y. Moriya, M. Kodera, T. Hisatomi, T. Minegishi, M. Katayama, K. Domen, *Chem. Mater.* **2016**, 28, 6869.
- [19] S. Wei, S. Jin, G. Pan, Z. Li, G. Liu, X. Xu, *J. Am. Ceram. Soc.* **2019**, 102, 6194.
- [20] N. C. Hildebrandt, J. Soldat, R. Marschall, *Small* **2015**, 11, 2051.
- [21] A. Bloesser, P. Voepel, M. O. Loeh, A. Beyer, K. Volz, R. Marschall, *J. Mater. Chem. A* **2018**, 6, 1971.
- [22] S. Pagola, G. Polla, G. Leyva, M. T. Casais, J. A. Alonso, R. Rasines, R. E. Carbinio, *Mater. Sci. Forum* **1996**, 819, 228.
- [23] A. Bloesser, R. Marschall, *ACS Appl. Energy Mater.* **2018**, 1, 2520.
- [24] K. Kawashima, M. Hojamberdiev, H. Wagata, K. Yubuta, S. Oishi, K. Teshima, *Cryst. Growth Des.* **2015**, 15, 333.
- [25] M. Davi, F. Schrader, T. Scholz, Z. Ma, A. Rokicinska, R. Dronskowski, P. Kustrowski, A. Slabon, *ACS Appl. Nano Mater.* **2018**, 1, 869.
- [26] Y. Suemoto, Y. Masubuchi, Y. Nagamine, A. Matsutani, T. Shibahara, K. Yamazaki, S. Kikkawa, *Inorg. Chem.* **2018**, 57, 9086.
- [27] J. F. Moulder, W. F. Stickle, P. E. Sobol, K. D. Bomben, *Handbook of X-Ray Photoelectron Spectroscopy*, Physical Electronics Division, Perkin-Elmer Corporation, Eden Prairie, MN, USA **1993**.
- [28] M. K. Bahl, *J. Phys. Chem. Solids* **1975**, 36, 485.
- [29] Z. Yang, X. Lu, W. Tan, J. Zhao, D. Yang, Y. Yang, Y. He, K. Zhou, *Appl. Surf. Sci.* **2018**, 439, 1119.
- [30] Z. Weibin, W. Weidong, W. Xueming, C. Xinlu, Y. Dawei, S. Changle, P. Liping, W. Yuying, B. Li, *Surf. Interface Anal.* **2013**, 45, 1206.
- [31] D. D. Sarma, C. N. R. Rao, *J. Electron Spectros. Relat. Phenom.* **1980**, 20, 25.
- [32] A. Darlinski, J. Halbritter, *Surf. Interface Anal.* **1987**, 10, 223.
- [33] A. Darlinski, J. Halbritter, *Z. Anal. Chem.* **1987**, 329, 266.
- [34] K. S. Havey, J. S. Zabinski, S. D. Walck, *Thin Solid Films* **1997**, 303, 238.
- [35] S. Badrinarayanan, S. Sinha, *J. Appl. Phys.* **1991**, 69, 1141.
- [36] D. Simon, C. Perrin, P. Baillif, *C. R. Acad. Sci. Paris, Ser. C* **1976**, 283, 241.
- [37] M. C. Blanco López, G. Fourlaris, B. Rand, F. L. Riley, *J. Am. Ceram. Soc.* **1999**, 82, 1777.
- [38] B. S. Shaheen, A. M. Hafez, B. Murali, A. R. Kirmani, A. Amassian, O. F. Mohammed, N. K. Allam, *Sol. Energy Mater. Sol. Cells* **2016**, 151, 149.
- [39] A. Rachel, S. G. Ebbinghaus, M. Güngerich, P. J. Klar, J. Hanss, A. Weidenkaff, A. Reller, *Thermochim. Acta* **2005**, 438, 134.
- [40] Y.-l. Cen, J.-j. Shi, M. Zhang, M. Wu, J. Du, W.-h. Guo, Y.-h. Zhu, *J. Colloid Interface Sci.* **2019**, 546, 20.
- [41] H. Wolff, R. Dronskowski, *J. Comput. Chem.* **2008**, 29, 2260.
- [42] A. Hofmann, M. Weiss, R. Marschall, *J. Phys. Energy* **2021**, 3, 014002.
- [43] A. S. Cherevan, L. Deilmann, T. Weller, D. Eder, R. Marschall, *ACS Appl. Energy Mater.* **2018**, 1, 5787.
- [44] F. Zhang, A. Yamakata, K. Maeda, Y. Moriya, T. Takata, J. Kubota, K. Teshima, S. Oishi, K. Domen, *J. Am. Chem. Soc.* **2012**, 134, 43.
- [45] H. Okamoto, M. Kodera, T. Hisatomi, M. Katayama, T. Minegishi, K. Domen, *Catal. Today* **2020**, 354, 204.
- [46] J. Rodríguez-Carvajal, *Phys. B* **1993**, 192, 55.
- [47] S. J. Clarke, K. A. Hardstone, C. W. Michie, M. J. Rosseinsky, *Chem. Mater.* **2002**, 14, 2664.
- [48] S. M. Antao, I. Hassan, *Phys. Chem. Miner.* **2007**, 34, 573.
- [49] R. J. Cernik, M. Barwick, F. Azough, R. Freer, *J. Appl. Crystallogr.* **2007**, 40, 749.
- [50] U. Lehmann, H. Müller-Buschbaum, *Z. Anorg. Allg. Chem.* **1980**, 471, 85.
- [51] C. D. Ling, M. Avdeev, R. Kuttan, V. V. Kharton, A. A. Yaremchenko, S. Fialkova, N. Sharma, R. B. Macquart, M. Hoelzel, M. Gutmann, *Chem. Mater.* **2009**, 21, 3853.